catalysts

MDPI

Article

Hg^0 Removal by a Palygorskite and Fly Ash Supported MnO_2-CeO_2 Catalyst at Low Temperature

Junwei Wang [1], Caihong Jiang [1], Liming Shi [2], Zhifeng Xue [2], Xie Wang [1,*], Can Xu [1], Xianlong Zhang [3,*] and Jianli Zhang [4]

[1] College of Chemistry and Chemical Engineering, Anqing Normal University, Anqing 246011, China; wangjunweilotus@163.com (J.W.); 1798087033@aqnu.edu.cn (C.J.); xucan@aqnu.edu.cn (C.X.)
[2] Development and Planning Department, Quality Control Center, Anqing Petrochemical Company, SINOPEC, Anqing 246002, China; shilm.aqsh@sinopec.com (L.S.); xuezf.aqsh@sinopec.com (Z.X.)
[3] School of Chemistry and Chemical Engineering, Hefei University of Technology, Hefei 230009, China
[4] State Key Laboratory of High-Efficiency Utilization of Coal and Green Chemical Engineering, Ningxia University, Yinchuan 750021, China; zhangjl@nxu.edu.cn
* Correspondence: anhuiss@sina.com (X.W.); zhangxianlong@hfut.edu.cn (X.Z.)

Abstract: MnO_2-CeO_2/PG-FA catalysts were prepared by supporting MnO_2-CeO_2 to PG-FA and used to remove Hg^0 in simulated flue gas. The results show that MnO_2-CeO_2/PG-FA catalyst had excellent and stable Hg^0 removal activity, which was mainly due to the combination effect of the catalytic oxidation activity by MnO_2-CeO_2 and the adsorption ability by PG-FA. Mn8-Ce0.5/PG-FA (with 8.0% MnO_2 and 0.5% CeO_2 loading) catalyst showed the highest Hg^0 removal efficiency at 140 °C and Hg^0 removal efficiency could be maintained above 95% with the space velocity of 6000 h^{-1} and Hg^0 concentration of 160 $\mu g/m^3$. O_2 promoted Hg^0 removal by MnO_2-CeO_2/PG-FA catalyst, while SO_2 and H_2O had inhibitory effects. In the presence of O_2, the inhibitory effect of SO_2 and H_2O can be obviously weakened. MnO_2-CeO_2/PG-FA catalysts were characterized with scanning electron microscope (SEM), X-ray diffraction (XRD), X-ray photoelectron spectroscopy (XPS) and temperature-programmed desorption experiments (TPD). The results of SEM and XRD showed that the active components MnO_2-CeO_2 dispersed well on the surface of PG-FA support. The results of XPS and TPD show that the Hg^0 removal process over MnO_2-CeO_2/PG-FA catalyst included adsorption and oxidation, HgO and $HgSO_4$ were generated and adsorbed on the catalyst. MnO_2-CeO_2/PG-FA catalyst also showed excellent regeneration performance after Hg^0 removal.

Keywords: palygorskite; fly ash; MnO_2; CeO_2; mercury; flue gas

Citation: Wang, J.; Jiang, C.; Shi, L.; Xue, Z.; Wang, X.; Xu, C.; Zhang, X.; Zhang, J. Hg^0 Removal by a Palygorskite and Fly Ash Supported MnO_2-CeO_2 Catalyst at Low Temperature. *Catalysts* **2022**, *12*, 662. https://doi.org/10.3390/catal12060662

Academic Editors: Boxiong Shen and Peng Yuan

Received: 24 May 2022
Accepted: 13 June 2022
Published: 16 June 2022

1. Introduction

Mercury emission from coal combustion has become an important source of environmental mercury pollution and caused a worldwide concern due to its toxicity, bioaccumulation and persistence in the food chain and the ecological environment [1,2]. Governments around the world have successively promulgated laws and regulations to limit mercury emissions from coal-fired power plants. Currently, more than 140 countries and regions have signed The Minamata Convention on Mercury treaty to limit mercury emission and use [3].

Generally, there are three main forms of Hg in coal-fired flue gas: gaseous Hg^0 (Hg^0_g), gaseous Hg^{2+} (Hg^{2+}_g) and Hg_p adsorbed on fly ash. Among them, Hg^{2+}_g is soluble in water and can be easily removed by wet dust removal device or wet flue gas desulfurization device. Hg_p can be removed by dust removal device along with fly ash. Hg^0, however, is difficult to remove by existing pollutant control devices due to its high volatility and insolubility in water [4]. Therefore, Hg^0 is the main mercury form released to the atmosphere and becomes the focus and difficulty of mercury pollution control in coal-fired flue gas.

Activated carbon injection (ACI) technology has been widely studied and applied to remove mercury in coal-fired flue gas [5–7]. However, the application of ACI technology in coal-fired power plants showed that several questions must be solved. The disadvantages of ACI are the short contact time between activated carbon and flue gas, poor capacity and incapability to regenerate activated carbon, leading to high cost and its limited application [8]. Obviously, developing economical and effective Hg removal technology is required.

It was reported that metal oxides had high catalytic oxidation activity for Hg^0, including V_2O_5, MnO_2, CeO_2, CuO, Mo_3O_4, etc., [9–18]. Among them, MnO_2 showed high activity for Hg^0 oxidation at low temperature. CeO_2, as a variable valence oxide (Ce^{4+}/Ce^{3+}), had excellent oxygen storage and release functions. It also showed good oxidation activity and a certain anti-SO_2 poisoning ability. Meanwhile, palygorskite, as a natural porous chain-layered water-containing magnesium-rich aluminum silicate clay mineral, has a certain adsorption ability with thermal stability and can be used as good catalyst supports [19,20]. In this paper, a palygorskite (PG) and fly ash (FA) supported MnO_2 and CeO_2 catalyst (MnO_2-CeO_2/PG-FA) was prepared and used to remove Hg^0 in simulated flue gas. The effect of MnO_2-CeO_2 loading, reaction temperature, flue gas components on Hg^0 removal and the speciation of Hg adsorbed over MnO_2-CeO_2/PG-FA were studied, as well as the regeneration of MnO_2-CeO_2/PG-FA after Hg^0 removal.

2. Results and Discussion

2.1. Characterization of the MnO_2-CeO_2/PG-FA Catalyst

Figure 1 shows the XRD results of PG-FA, Mn8/PG-FA, Ce0.5/PG-FA and Mn8Ce0.5/PG-FA catalysts. It can be seen that there were obvious peaks for $Al_6Si_2O_{13}$ (JPCDS 15-0776), $(Mg, Al)_5(Si, Al)_8O_{20}(OH)_2 \bullet 8H_2O$ (JPCDS 21-0958) and SiO_2 (JPCDS 46-1045) in PG-FA support. The XRD pattern of Ce0.5/PG-FA catalyst was completely consistent with the PG-FA support and no CeO_2 peak has been observed, which was mainly due to the low loading amount of CeO_2. Compared to the PG-FA support, the Mn8/PG-FA catalyst and Mn8Ce0.5/PG-FA catalyst showed MnO_2 peaks (JPCDS 24-0735), indicating that MnO_2 was successfully supported onto PG-FA support.

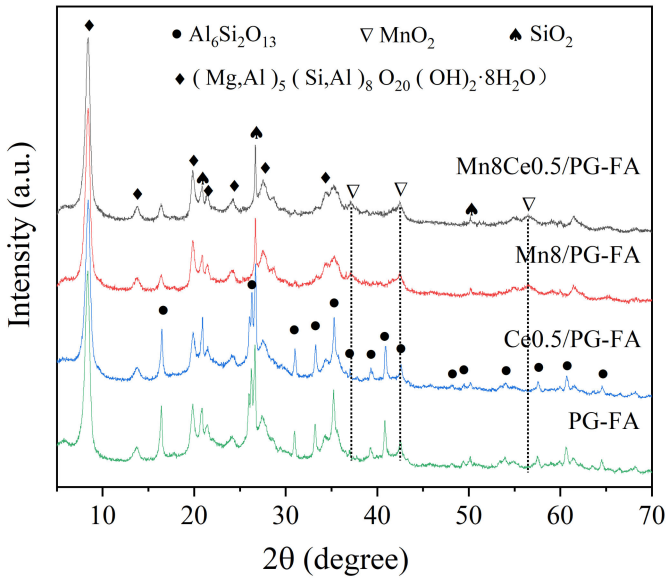

Figure 1. XRD characterization of PG-FA, Mn8/PG-FA, Ce0.5/PG-FA and MnO_2-CeO_2/PG-FA catalysts.

Figure 2 shows the SEM images of Mn8-Ce0.5/PG-FA catalyst. It can be seen that Mn8-Ce0.5/PG-FA catalyst had an obvious porous structure, which was facilitated for the diffusion of flue gas in catalyst particles. Besides, PG-FA support had a specific surface

area of 100.99 m^2/g, and it was beneficial to the loading and dispersion of MnO_2 and CeO_2 components, as well as the enhancement of adsorption capacity of catalysts.

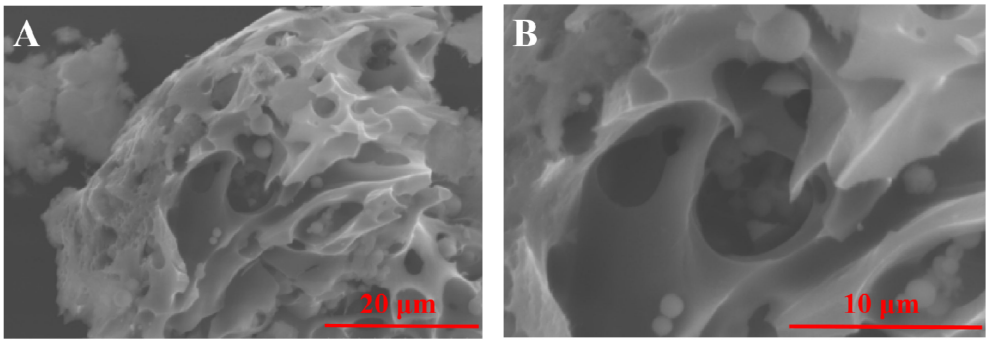

Figure 2. SEM images of the Mn8-Ce0.5/PG-FA catalyst (**A**: × 2.0 k, **B**: × 5.0 k).

2.2. Effect of MnO_2 and CeO_2 Loading on Hg^0 Removal

Figure 3 shows Hg^0 removal by MnO_2-CeO_2/PG-FA catalysts with different MnO_2 and CeO_2 loading at 140 °C in simulated flue gas (5% O_2, 5% H_2O, 0.15% SO_2, balance N_2, $C_{Hg}{}^0$ = 160 μg/m^3) for 5 h. It can be seen that PG-FA had low Hg^0 removal capability and Hg^0 removal efficiency was only about 50%. Supporting single 8% MnO_2 and 0.5% CeO_2 could obviously improve Hg^0 removal capability, and Hg^0 removal efficiency reached 90% and 83% for Mn8/PG-FA and Ce0.5/PG-FA, respectively. Supporting MnO_2-CeO_2 onto PG-FA further improved Hg^0 removal capability, and Mn8-Ce0.5/PG-FA had the highest Hg^0 removal capability and Hg^0 removal efficiency was above 98%. Compared to single MnO_2 and CeO_2 catalyst, MnO_2-CeO_2 bimetallic catalyst had a higher Hg^0 removal capability, which was mainly due to the co-effects of oxidation activity of MnO_2 and CeO_2, as well as the anti-SO_2 ability of CeO_2. Although the specific surface area of the Mn8/PG-FA and Mn8-Ce0.5/PG-FA catalyst decreased slightly after MnO_2 and CeO_2 loading, Hg^0 removal capability still improved. The high Hg^0 removal capability of MnO_2-CeO_2/PG-FA was mainly due to the oxidation activity of MnO_2 and CeO_2 for Hg^0, as well as the adsorption ability of PG-FA. This was similar to Hg^0 capture by V_2O_5/AC catalyst and MnO_x/PG catalyst in our previous researches [20,21].

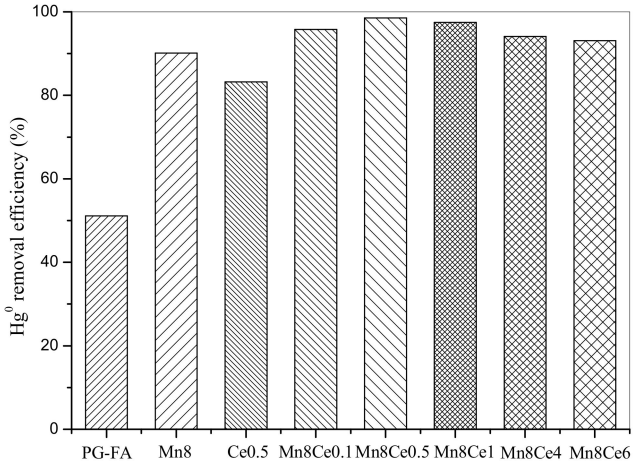

Figure 3. Hg^0 removal by MnO_2-CeO_2/PG-FA catalysts. (reaction conditions: 5% O_2, 5% H_2O, 0.15% SO_2, balance N_2, $C_{Hg}{}^0$ = 160 μg/m^3, GHSV = 6000 h^{-1}, T = 140 °C).

2.3. Effect of Temperature on Hg^0 Removal by MnO_2-CeO_2/PG-FA

Figure 4 shows Hg^0 removal by PG-FA and Mn8-Ce0.5/PG-FA at different temperatures. It can be seen that Hg^0 removal capability of PG-FA decreased as the temperature increased, which was mainly due to the decrease of adsorption effect by PG-FA for Hg^0

removal. Mn8-Ce0.5/PG-FA showed high Hg^0 removal capability in the temperature range of 120 to 200 °C, and Hg^0 removal efficiencies were still above 85% after 280 min. Hg^0 removal efficiency increased firstly and then decreased as the temperature increased from 120 to 200 °C, and the highest was at 140 °C. Since Hg^0 removal process included oxidation and adsorption, the trend of Hg^0 removal efficiency indicated that the effect extent of oxidation and adsorption on Hg^0 removal over Mn8-Ce0.5/PG-FA was different at different temperatures [21]. The co-effect was the highest at 140 °C leading to the highest Hg^0 removal efficiency.

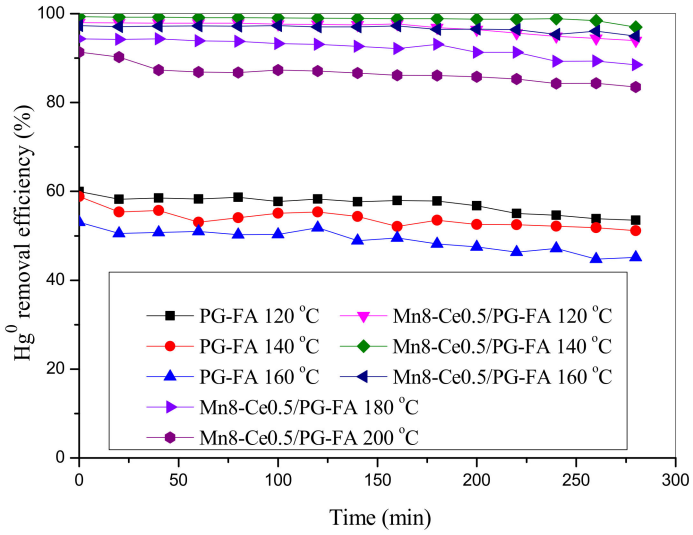

Figure 4. Effect of temperature on Hg^0 removal by PG-FA and Mn8-Ce0.5/PG-FA. (reaction conditions: 5% O_2, 5% H_2O, 0.15% SO_2, balance N_2, $C_{Hg}{}^0$ = 160 μg/m^3, GHSV = 6000 h^{-1}).

2.4. Effect of Flue Gas Components on Hg^0 Removal by MnO_2-CeO_2/PG-FA

Figure 5 shows the effects of flue gas components on Hg^0 removal over Mn8-Ce0.5/PG-FA. It can be seen that O_2 had a promotion effect while SO_2 and H_2O showed an inhibition effect, which may be due to the competitive adsorption between Hg^0 and SO_2 or H_2O. However, in the presence of O_2, Hg^0 removal efficiency increased slightly, indicating that O_2 offset the inhibition effect of SO_2 and H_2O to a certain extent. Since Hg^0 oxidation was mainly due to the lattice oxygen of metal oxides, the role of O_2 was to resume the oxidation activity of MnO_2-CeO_2 by replenishing O to the used MnO_2-CeO_2 sites after Hg^0 oxidation [20–22]. Furthermore, in the presence of O_2, SO_2 and H_2O, Hg^0 was oxidized to form $HgSO_4$ as shown in Figure 6.

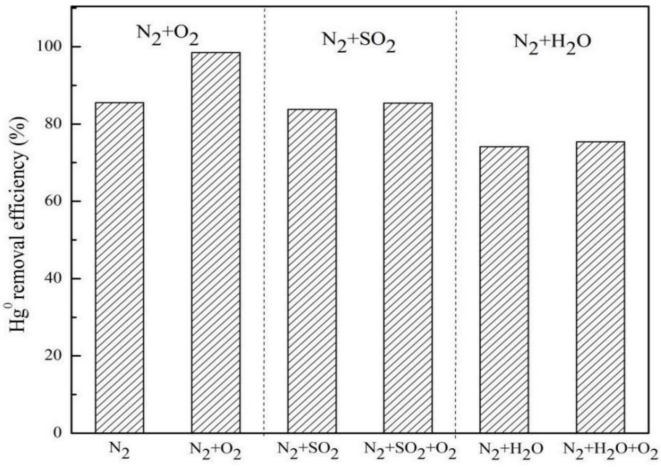

Figure 5. Effect of flue gas components on Hg^0 removal by Mn8-Ce0.5/PG-FA (reaction conditions: $C_{Hg}{}^0$ = 160 μg/m^3, GHSV = 6000 h^{-1}, T = 140 °C).

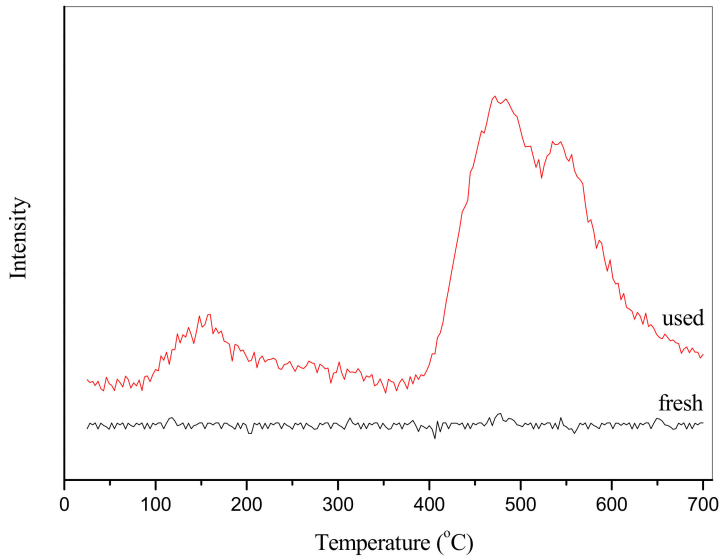

Figure 6. Hg release of the fresh and used Mn8-Ce0.5/PG-FA samples during TPD process.

2.5. Speciation of Hg Adsorbed over Mn8-Ce0.5/PG-FA

Temperature programmed desorption (TPD) experiments were conducted to identify the speciation of Hg adsorbed over Mn8-Ce0.5/PG-FA. Mn8-Ce0.5/PG-FA was firstly used to remove Hg^0 in N_2 + O_2 + SO_2 + H_2O at 140 °C for 5 h and then was used for TPD experiments. Figure 6 shows the Hg release behaviors of the fresh and used Mn8-Ce0.5/PG-FA catalysts upon heating to 700 °C in Ar. It can be seen that the fresh Mn8-Ce0.5/PG-FA sample showed no Hg release during the TPD process. As for the used Mn8-Ce0.5/PG-FA sample, however, it showed three obvious Hg release peaks at about 150 °C, 480 °C and 540 °C, which could be attributed to Hg^0, HgO and $HgSO_4$, respectively [23–26]. This indicated that the speciation of Hg adsorbed over Mn8-Ce0.5/PG-FA was mainly Hg^{2+} compounds, confirming the oxidation of Hg^0 to Hg^{2+} by MnO_2 and CeO_2, as well as the reaction of Hg^0 with O_2 and SO_2 to form $HgSO_4$.

XPS analyses were also conducted to identify the speciation of Hg adsorbed over Mn8-Ce0.5/PG-FA. Figure 7 shows the results of Mn 2p, Ce 3d and Hg 4f for fresh and used MnO_2-CeO_2/PG-FA catalyst. Compared to the fresh MnO_2-CeO_2/PG-FA sample, the amount of Mn^{4+} (643.4 eV for Mn $2p_{2/3}$ and 655.2 eV for Mn $2p_{1/3}$) and Ce^{4+} (u, u^2, u^3, v, v^2, v^3) decreased while Mn^{3+} (642.3 eV for Mn $2p_{2/3}$ and 654.1 eV for Mn $2p_{1/3}$) and Ce^{3+} (u^1, v^1) increased for the used MnO_2-CeO_2/PG-FA sample. Besides, it can be seen in Figure 7E that there was a peak at around 99.8 eV for the fresh MnO_2-CeO_2/PG-FA catalyst, which could be attributed to the SiO_2 of PG support [20,27]. As for the used MnO_2-CeO_2/PG-FA catalyst after Hg^0 removal, a new peak at around 101.1 eV appeared (Figure 7F), which could be ascribe to Hg^{2+} of HgO and $HgSO_4$ [18,22]. These results confirm the reaction of Hg^0 with MnO_2 and CeO_2, i.e., Hg^0 was oxidized to Hg^{2+} while O of MnO_2-CeO_2 was consumed and Mn^{4+}, Ce^{4+} were reduced to Mn^{3+}, Ce^{3+}. Meanwhile, adsorbed O_2 could replenish oxygen for Mn^{3+}, Ce^{3+} to form MnO_2 and CeO_2 to resume their oxidation activity [21,22].

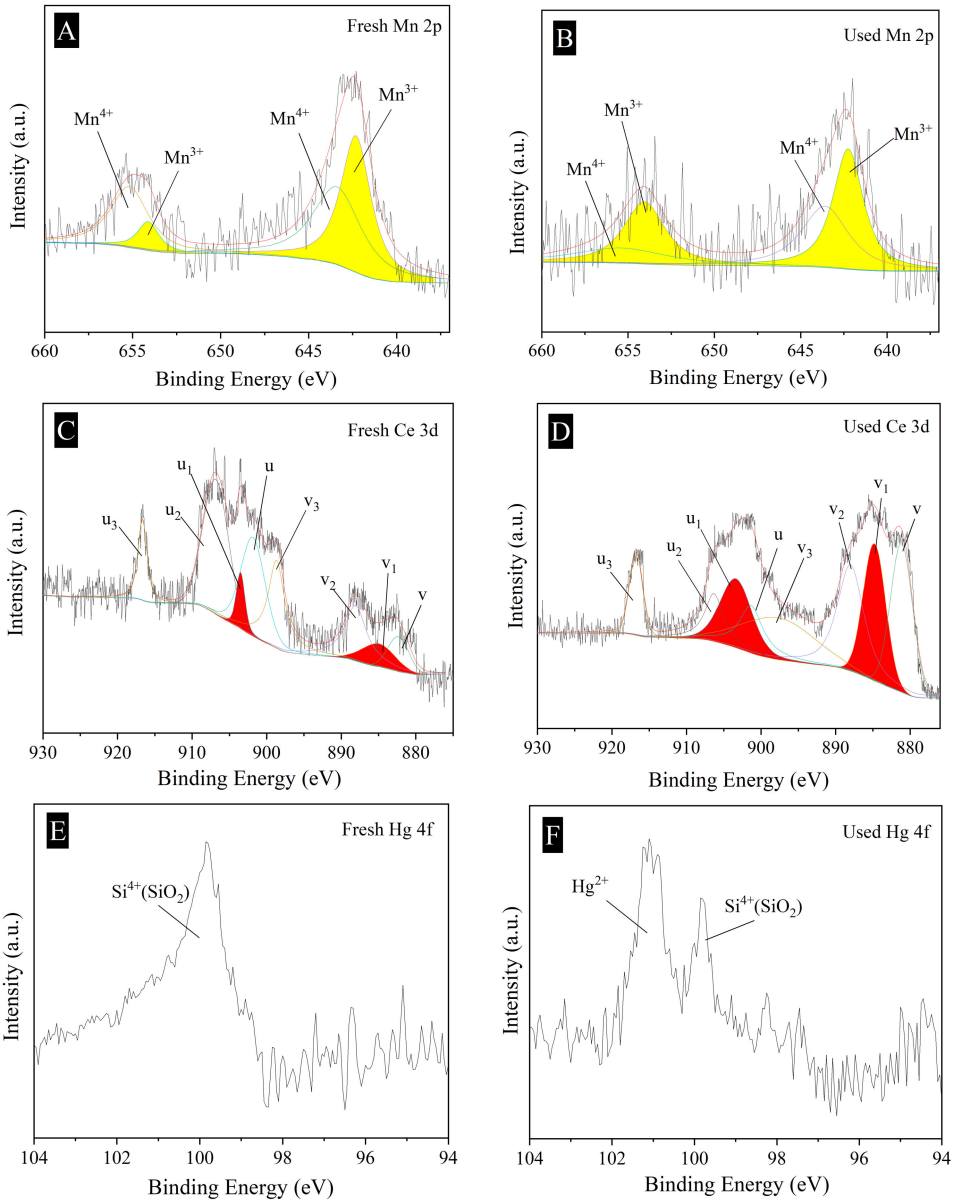

Figure 7. XPS spectra of Mn 2p (**A**,**B**), Ce 3d (**C**,**D**) and Hg 4f (**E**,**F**) over fresh and used Mn8-Ce0.5/PG-FA catalyst.

2.6. Hg^0 Removal Process over MnO_2-CeO_2/PG-FA Catalyst

Based on the above experiments and characterization results, Hg^0 removal over MnO_2-CeO_2/PG-FA catalyst might include adsorption and oxidation. Hg^0 removal process over MnO_2-CeO_2/PG-FA can be summarized as follows and Figure 8:

Hg^0 (g) → Hg^0 (ad)
O_2 (g) → 2[O] (ad)
$2CeO_2$ → Ce_2O_3 + [O]
$2MnO_2$ → Mn_2O_3 + [O]
Hg^0 (ad) + [O] → HgO (ad)
SO_2 (g) + [O] → SO_3 (ad)
Hg^0 (ad) + SO_3 (ad) + [O] → $HgSO_4$ (ad)
SO_3 (ad) + HgO (ad) → $HgSO_4$ (ad)
SO_3 (ad) + H_2O (ad) → H_2SO_4 (ad)
H_2SO_4 (ad) + HgO (ad) → $HgSO_4$ (ad) + H_2O (ad)

$Ce_2O_3 + [O] \rightarrow 2CeO_2$
$Mn_2O_3 + [O] \rightarrow 2MnO_2$

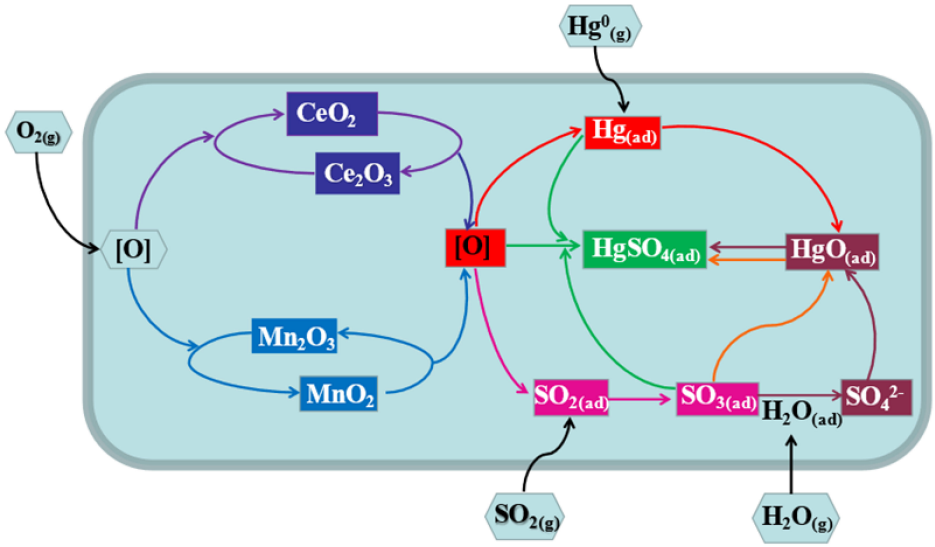

Figure 8. Reactions of Hg^0 over MnO_2-CeO_2/PG-FA.

2.7. Regeneration of MnO_2-CeO_2/PG-FA Catalyst after Hg^0 Removal

The above results show that MnO_2-CeO_2/PG-FA catalyst had an excellent Hg^0 removal capability at low temperature. To investigate the reusability of MnO_2-CeO_2/PG-FA catalyst, the Mn8-Ce0.5/PG-FA after Hg^0 removal for 60 h with Hg^0 removal efficiency of 76% was regenerated and reused for Hg^0 removal again. The results of Mn8-Ce0.5/PG-FA, Mn8-Ce0.5/PG-FA-Re-400 °C and Mn8-Ce0.5/PG-FA-Re-500 °C for Hg^0 removal are shown in Figure 9. It can be seen that the regenerated MnO_2-CeO_2/PG-FA catalyst still had a high and stable capability for Hg^0 removal. Hg^0 removal efficiency of Mn8-Ce0.5/PG-FA-Re-400 °C and Mn8-Ce0.5/PG-FA-Re-500 °C were still above 90% and 85% after 280 min, respectively. As the regeneration temperature increased from 400 to 500 °C, Hg^0 removal efficiency decreased slightly. This may be due to the change of structure and chemical properties of MnO_2-CeO_2/PG-FA during regeneration, causing pores blockage and partial active sites loss on the surface of MnO_2-CeO_2/PG-FA catalyst at higher regeneration temperature. The MnO_2-CeO_2/PG-FA catalyst had excellent Hg^0 removal activity and regeneration performance.

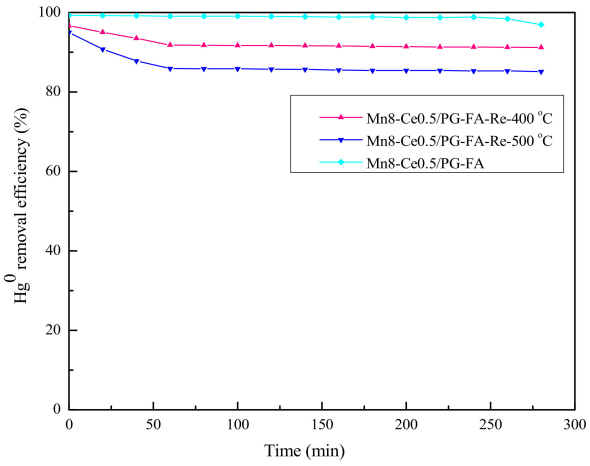

Figure 9. Comparison of Hg^0 removal by Mn8-Ce0.5/PG-FA, Mn8-Ce0.5/PG-FA-Re-400 °C and Mn8-Ce0.5/PG-FA-Re-500 °C (reaction conditions: 5% O_2, 5% H_2O, 0.15% SO_2, balance N_2, C_{Hg^0} = 160 μg/m^3, GHSV = 6000 h^{-1}, T = 140 °C).

3. Materials and Methods

3.1. Catalysts Preparation

The PG and fly ash were mixed at a ratio (3:7), and then mixed with distilled water in a certain proportion (1 g:1.5 mL), dried at 110 °C for 6 h, then calcined at 300 °C for 6 h in air. Table 1 shows the compositions of PG and FA. The obtained PG-FA samples were crushed and screened into 40–60 mesh. MnO_2-CeO_2/PG-FA catalysts were prepared by pore volume impregnation of PG-FA with an $Mn(NO_3)_2$ and $Ce(NO_3)_3$ aqueous solution (1 g:1.2 mL). According to the loading amount of MnO_2-CeO_2 in the prepared MnO_2-CeO_2/PG-FA catalyst, the FA-PG support was impregnated in an equal volume with 0.1650 g/mL of $Mn(NO_3)_2$ and 0.0095 g/mL $Ce(NO_3)_3$ solution. After impregnating, it was stewed at room temperature for 8 h, dried at 50 °C for 5 h and at 110 °C for 5 h in air. Then it was calcined at 300 °C for 3 h in air. Several MnO_2-CeO_2/PG-FA catalysts with different MnO_2-CeO_2 loading (wt.%) were prepared and named according to the weight percentage of MnO_2-CeO_2 in MnO_2-CeO_2/PG-FA. For example, Mn8-Ce0.5/PG-FA referred to MnO_2-CeO_2/PG-FA catalyst containing 8.0% MnO_2 and 0.5% CeO_2. Table 2 shows the properties of the PG-FA support, Mn8/PG-FA and Mn8-Ce0.5/PG-FA catalyst.

Table 1. The main chemical compositions of PG and FA.

Sample	Chemical Compositions							
	SiO_2	**Al_2O_3**	**Fe_2O_3**	**CaO**	**MgO**	**TiO_2**	**K_2O**	**MnO**
PG	69.45	11.84	5.14	0.21	12.17	0.44	0.51	0.05
FA	48.29	21.64	3.05	20.33	1.74	0.98	1.66	0.04

Table 2. Characterization of textural properties of the samples.

Sample	BET Area (m^2/g)	Micropore Volume (cm^3/g)	Average Diameter (nm)
PG-FA	100.99	0.35	13.86
Mn8/PG-FA	91.22	0.31	13.59
Mn8-Ce0.5/PG-FA	87.63	0.28	11.06

3.2. Hg^0 Removal by MnO_2-CeO_2/PG-FA Catalyst

Hg^0 removal experiments by MnO_2-CeO_2/PG-FA catalyst were carried out in a fixed-bed quartz reactor as shown in Figure 10. 0.5 g MnO_2-CeO_2/PG-FA catalyst was used for each experiment at 120–200 °C in simulated flue gas containing 5% O_2, 5% H_2O, 0.15% SO_2, 160 μg/m^3 Hg^0 and balance N_2. The total flow rate was 100 mL/min, corresponding to a space velocity of about 6000 h^{-1}. Hg^0 was generated by an Hg^0 permeation tube (VICI Metronics) immerged in a water bath. The whole gas tube for Hg^0 delivery was kept at 120 °C to avoid the adsorption of Hg^0. The Hg^0 concentration in the inlet and outlet gas of the reactor was continuously measured by a RA-915M mercury analyzer (Lumex Instruments, Russia). Hg^0 removal efficiency was defined as follows:

$$E_{Hg}(\%) = \frac{C_0 - C_1}{C_0} \times 100\%$$

where C_0 and C_1 represent the Hg^0 concentration at the inlet and outlet gas of the reactor, respectively.

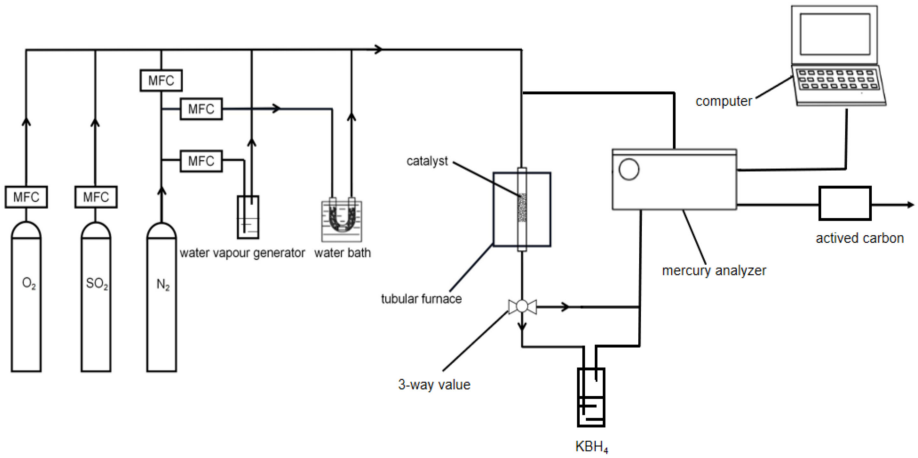

Figure 10. Schematic diagram of Hg^0 removal by MnO_2-CeO_2/PG-FA.

3.3. Catalyst Regeneration

The used MnO_2-CeO_2/PG-FA catalyst after Hg^0 removal was thermally regenerated in the fixed bed reactor in Figure 10. The sample was firstly heated to the regeneration temperature (300–500 °C) and maintain for 2 h in N_2, and then was heated at 350 °C for 2 h in an air atmosphere. After the regenerated MnO_2-CeO_2/PG-FA catalyst was naturally cooled to room temperature, simulated flue gas was switched and the regenerated MnO_2-CeO_2/PG-FA was used to remove Hg^0 again.

3.4. Characterization

The N_2 adsorption-desorption tests were carried out by an Autosorb-iQ analyzer (Quantachrome, Boynton Beach, FL, USA). The specific surface areas were calculated by the Brunauer-Emmett-Teller (BET) method, the pore structure parameters were analyzed by the Barrett-Joyner-Halenda (BJH) method.

The morphologies of the MnO_2-CeO_2/PG-FA catalysts were performed on a scanning electron microscope (SEM) (JSM-7001F, JEOL, Akishima City, Japan).

The crystal phase structure of the MnO_2-CeO_2/PG-FA catalysts were characterized by XRD diffractometer (D8-ADVANCE-A25, Bruker, Karlsruhe, Germany), using Cu Kα rays and 10–80° scanning range. XRD diffraction data adopt step scan method (0.02°).

The X-ray photoelectron spectroscopy (XPS) analysis was performed on an ESCALAB 250Xi spectrometer (Thermo Fisher, Waltham, MA, USA) using an Al Kα X-ray source at room temperature. All binding energies (BE) were adjusted with the C 1s binding energy value of 284.6 eV.

Temperature-programmed desorption (TPD) experiments were conducted in a quartz tube reactor using 0.1 g sample. The sample was firstly used to remove Hg^0 at 140 °C for 280 min, then cooled to the room temperature and swept with N_2 for 20 min, finally heated from room temperature to 700 °C with a heating rate of 10 °C/min. The outlet gas from the reactor was introduced into a KBH_4 solution to reduce the possibly existing Hg^{2+} to Hg^0. The Hg^0 concentration in the effluent gas after the KBH_4 solution was continuously measured by an on-line mercury analyzer (RA-915M, Lumex, St. Petersburg, Russia).

4. Conclusions

MnO_2-CeO_2/PG-FA catalyst had excellent Hg^0 removal activity and stability, which was mainly due to the combination effect of the catalytic oxidation activity by MnO_2-CeO_2 and adsorption ability by PG-FA. Hg^0 was oxidized to form HgO and $HgSO_4$, and then adsorbed on the MnO_2-CeO_2/PG-FA catalyst. The porous structure of the support PG-FA was conducive to the dispersion of the active component MnO_2-CeO_2 and the adsorption and oxidation of Hg^0. Mn8-Ce0.5/PG-FA catalyst showed the highest Hg^0 removal efficiency at 140 °C. O_2 exhibited a promoting effect on Hg^0 removal, while SO_2

and H_2O showed an obvious inhibitory effect. Hg^0 removal over MnO_2-CeO_2/PG-FA catalyst included adsorption, oxidation and reaction. The used Mn8-Ce0.5/PG-FA catalyst after Hg^0 removal can be regenerated and its capability for Hg^0 removal can be effectively recovered, and the Mn8-Ce0.5/PG-FA-Re-400 °C catalyst showed excellent Hg^0 removal activity and regeneration performance.

Author Contributions: Conceptualization, J.W. and X.Z.; methodology, C.J. and C.X.; validation, X.Z. and J.Z.; formal analysis, X.W.; investigation, L.S.; resources, J.W.; data curation, C.J.; writing—original draft preparation, J.W. and C.X.; writing—review and editing, X.W.; supervision, Z.X.; funding acquisition, J.W. and X.W. All authors have read and agreed to the published version of the manuscript.

Funding: This research was funded by the financial support from the National Natural Science Foundation of China (21203003, 51404014), Foundation of State Key Laboratory of High-efficiency Utilization of Coal and Green Chemical Engineering (2020-KF-28) and Anhui Provincial Discipline (Professional) Top Talent Academic Funding Project (gxbjZD2021062) and Natural Science Foundation of Anhui Education Department (KJ2019A0558) and open fund of AnHui Province Key Laboratory of Optoelectronic and Magnetism Functional Materials (ZD 2021004).

Data Availability Statement: Raw data are available from the corresponding author upon request.

Conflicts of Interest: The authors declare no conflict of interest.

References

1. Yang, L.X.; Zhang, Y.Y.; Wang, F.F.; Luo, Z.D.; Guo, S.J.; Strähle, U. Toxicity of mercury: Molecular evidence. *Chemosphere* **2020**, *245*, 125586. [CrossRef] [PubMed]
2. Wang, J.C.; Li, D.K.; Ju, F.L.; Han, L.N.; Chang, L.P.; Bao, W.R. Supercritical hydrothermal synthesis of zeolites from coal fly ash for mercury removal from coal derived gas. *Fuel Process. Technol.* **2015**, *136*, 96–105.
3. Bank, M.S. The mercury science-policy interface: History, evolution and progress of the Minamata Convention. *Sci. Total Environ.* **2020**, *722*, 137832–137837. [CrossRef] [PubMed]
4. Li, B.; Wang, H.L. Effect of flue gas purification facilities of coal-fired power plant on mercury emission. *Energy Rep.* **2021**, *7*, 190–196. [CrossRef]
5. Sjostrom, S.; Durham, M.; Bustard, C.J.; Martin, C. Activated carbon injection for mercury control: Overview. *Fuel* **2010**, *89*, 1320–1322. [CrossRef]
6. Liu, H.; Chang, L.; Liu, W.J.; Xiong, Z.; Zhao, Y.C.; Zhang, J.Y. Advances in mercury removal from coal-fired flue gas by mineral adsorbents. *Chem. Eng. J.* **2020**, *379*, 122263.
7. Takaoka, M.; Cheng, Y.C.; Oshit, K.; Watanabe, T.; Eguchi, S. Mercury removal from the flue gases of crematoria via pre-injection of lime and activated carbon into a fabric filter. *Process Saf. Environ.* **2021**, *148*, 323–332. [CrossRef]
8. Wu, H.Y.; Li, C.T.; Zhao, L.K.; Zhang, J.; Zeng, G.M.; Xie, Y.E.; Zhang, X.N.; Wang, Y. Removal of gaseous elemental mercury by cylindrical activated coke loaded with CoO_X-CeO_2 from simulated coal combustion flue gas. *Energy Fuels* **2015**, *29*, 6747–6757.
9. Zhao, H.T.; Ezeh, C.I.; Yin, S.F.; Xie, Z.L.; Pang, C.H.; Zheng, C.H.; Gao, X.; Wu, T. MoO_3-adjusted δ-MnO_2 nanosheet for catalytic oxidation of Hg^0 to Hg^{2+}. *Appl. Catal. B* **2020**, *263*, 117829. [CrossRef]
10. Zhou, Z.J.; Liu, X.W.; Zhao, B.; Shao, H.Z.; Xu, Y.S.; Xu, M.H. Elemental mercury oxidation over manganese-based perovskite-type catalyst at low temperature. *Chem. Eng. J.* **2016**, *288*, 701–710.
11. Zhao, L.K.; Li, C.T.; Zhang, J.; Zhang, X.N.; Zhan, F.M.; Ma, J.F.; Xie, Y.E.; Zeng, G.M. Promotional effect of CeO_2 modified support on V_2O_5-WO_3/TiO_2 catalyst for elemental mercury oxidation in simulated coal-fired flue gas. *Fuel* **2015**, *153*, 361–369. [CrossRef]
12. Ye, D.; Wang, X.X.; Wang, R.X.; Wang, S.Y.; Liu, H.; Wang, H.N. Recent advances in MnO_2-based adsorbents for mercury removal from coal-fired flue gas. *J. Environ. Chem. Eng.* **2021**, *9*, 105993. [CrossRef]
13. Zhou, Q.; Tao, X.; Di, G.; Shang, Y.; Lu, P.; Xu, G.; Liu, M.; Zheng, Y.; Dong, L. Elemental mercury capture from flue gas by magnetic recyclable $Fe_6Mn_{1-x}Ce_xO_y$ sorbent. Part 1. Performance evaluation and regeneration. *Fuel* **2021**, *304*, 120723. [CrossRef]
14. Zhang, S.B.; Zhao, Y.C.; Yang, J.P.; Zhang, Y.; Sun, P.; Yu, X.H.; Zhang, J.Y.; Zheng, C.G. Simultaneous NO and mercury removal over MnO_x/TiO_2 catalyst in different atmospheres. *Fuel Process. Technol.* **2017**, *166*, 282–290. [CrossRef]
15. Yang, Y.J.; Liu, J.; Zhang, B.K.; Zhao, Y.C.; Chen, X.; Shen, F.H. Experimental and theoretical studies of mercury oxidation over CeO_2-WO_3/TiO_2 catalysts in coal-fired flue gas. *Chem. Eng. J.* **2017**, *317*, 758–765. [CrossRef]
16. Li, H.L.; Zhang, W.L.; Wang, J.; Yang, Z.Q.; Li, L.Q.; Shih, K. Coexistence of enhanced Hg^0 oxidation and induced Hg^{2+} reduction on CuO/TiO_2 catalyst in the presence of NO and NH_3. *Chem. Eng. J.* **2017**, *330*, 1248–1254. [CrossRef]
17. Zhao, B.; Liu, X.W.; Zhou, Z.J.; Shao, H.Z.; Xu, M.H. Catalytic oxidation of elemental mercury by Mn-Co/CNT at low temperature. *Chem. Eng. J.* **2016**, *284*, 1233–1241. [CrossRef]
18. Zhang, L.Y.; Yang, S.; Lai, Y.K.; Liu, H.; Fan, Y.; Liu, C.; Wang, H.Y.; Chai, L.Y. In-situ synthesis of monodispersed Cu_xO heterostructure on porous carbon monolith for exceptional removal of gaseous Hg^0. *Appl. Catal. B* **2020**, *265*, 118556. [CrossRef]

19. Zhang, X.L.; Wu, Q.; Diao, Q.C.; Wang, J.W.; Xiao, K.S.; Yang, B.J.; Wu, X.P. Performance study for NH_3-SCR at low temperature based on different methods of Mn_x/SEP catalyst. *Chem. Eng. J.* **2019**, *370*, 364–371. [CrossRef]
20. Wang, J.W.; Xu, C.; Qin, W.; Zhang, J.L.; Zhang, X.L.; Cui, X.F. Hg^0 removal by palygorskite (PG) supported MnO_x catalyst. *J. Fuel Chem. Technol.* **2020**, *48*, 1442–1451.
21. Wang, J.W.; Shen, Y.Y.; Dong, Y.J.; Qin, W.; Zhang, Q.P.; Lu, L.; Zhang, Y.G. Oxidation and adsorption of gas-phase Hg^0 over a V_2O_5/AC catalyst. *RSC Adv.* **2016**, *6*, 77553–77557. [CrossRef]
22. Zhu, Y.C.; Hou, Y.Q.; Wang, J.W.; Guo, Y.P.; Huang, Z.G.; Han, X.J. Effect of SCR atmosphere on the removal of Hg^0 by a V_2O_5-CeO_2/AC catalyst at low temperature. *Environ. Sci. Technol.* **2019**, *53*, 5521–5527.
23. Rumayor, M.; Diaz-Somoano, M.; López-Antón, M.A. Temperature programmed desorption as a tool for the identification of mercury fate in wet-desulphurization systems. *Fuel* **2015**, *148*, 98–103. [CrossRef]
24. Wu, S.J.; Uddin, M.; Nagano, S. Fundamental study on decomposition characteristics of mercury compounds over solid powder by temperature-programmed decomposition desorption mass spectrometry. *Energy Fuels* **2011**, *25*, 144–153. [CrossRef]
25. Uddin, M.A.; Ozaki, M.; Sasaoka, E.J.; Wu, S.J. Temperature-programmed decomposition desorption of mercury species over activated carbon sorbents for mercury removal from coal-derived fuel gas. *Energy Fuels* **2009**, *23*, 4710–4716. [CrossRef]
26. Liu, M.; Li, C.T.; Zeng, Q.; Du, X.Y.; Gao, L.; Li, S.H.; Zhai, Y.B. Study on removal of elemental mercury over MoO_3-CeO_2/cylindrical activated coke in the presence of SO_2 by Hg-temperature-programmed desorption. *Chem. Eng. J.* **2019**, *371*, 666–678. [CrossRef]
27. Wang, J.W.; Yang, J.L.; Liu, Z.Y. Gas-phase elemental mercury capture by a V_2O_5/AC catalyst. *Fuel Process. Technol.* **2010**, *91*, 676–680. [CrossRef]